Journal of the Brazilian Society of Mechanical Sciences and Engineering (2018) 40:236
https://doi.org/10.1007/s40430-018-1161-1

TECHNICAL PAPER

Digital image-stitching techniques applied to dynamic measurement of large structures

Danilo Damasceno Sabino[1] · Joao Antonio Pereira[1] · Peyman Poozesh[2]

Received: 29 November 2017 / Accepted: 27 March 2018 / Published online: 10 April 2018

Abstract
In this work has been discussed a propose of using three-dimensional point-tracking measuring technique for measurement of large structures in which the entire field of interest could not be captured by a unique stereo-vision system. Two pairs of a stereo-system are used to capture the whole field of measurement of interest of the model and point cloud registration techniques are exploited aiming at extending the capability of digital image measurement system for dynamic measuring (displacement) for large-scale structures. Three different image registration algorithms, principle component analysis, singular value decomposition, and iterative closest point are used in the stitching process to join the point clouds obtained with the multi-camera system. The proposal is applied to vibration measurement of a wind turbine blade of 2.3 m in length, whose field of view of the whole set of points of interest is greater than the field of view of a unique stereo-vision system. The reconstruction of the set of measured points was obtained from the junction of the points clouds of each stereo-system in a reference system and a probabilistic and statistical analysis of the error generated by the transformation of the point clouds was performed. And finally, the frequencies of the structure obtained from the digital image measured data were compared with the values obtained from a set of accelerometers.

Keywords Registration · 3DPT · Data stitching · Large structures · Wind turbine blades

1 Introduction

Instrumentation and measurement of long and complex structures are a challenge for experimental test engineering. Long and complex structures demand the use of many sensors when it is desired a good spatial resolution of the model, which is not always possible due to the needing of special instrumentation and acquisition systems which are very specifics and generally high costs. Thus, it is highly desirable to have more general and accessible measurement techniques for testing of long structures.

The use of traditional contact sensors, such as strain gauges and accelerometers, for inspection of long and complex structures, is a challenge, since they are punctual sensors, and consequently, a reliable inspection usually demands a large number of installed sensors, which involves large cable extensions that can induce noise in the measurement and even, in long and flexible structures, add mass to the structure. In this way, carrying out tests of long and complex structures becomes difficult using these sensors.

Non-contact sensors such as scanning laser Doppler vibrometer (SLDV) are also used for inspection of large structures, but also have limitations by doing the measurement in a punctual and sequential way, that is, they cannot measure all the points simultaneously. Therefore, the measurement must be repeated for each point. Moreover, when subjected to loads, the long structures may undergo deformations, generating large movements and consequently changing the position of the reading point of the sensor in the structure, which may compromise the measurement.

An alternative to these more traditional techniques is the use of stereophotogrammetry, which has been highlighted as very promising optical technique for dynamic

Technical Editor: Kátia Lucchesi Cavalca Dedini.

✉ Danilo Damasceno Sabino
danilosabino@hotmail.com

[1] Department of Mechanical Engineering, UNESP-Univ Estadual Paulista, Ilha Solteira, SP, Brazil

[2] University of Massachusetts Lowell, One University Ave., Lowell, MA 01854, USA

measurements [1–3], since it can be used to measure a set of points simultaneously (full field) and it is not so restrictive to large deformations [4]. In this technique, images captured from a stereo-pair of charge-coupled device (CCD) or complementary metal-oxide-semiconductor (CMOS) cameras, in a static condition or in a time sequence, are processed using either digital image correlation (DIC) or three-dimensional point-tracking (3DPT) techniques. The two techniques work on the principle of triangulation to determine the coordinates of an object by comparing at least two images recorded simultaneously of the same object from different angles of view. However, for large structures in both, indoor and outdoor areas, the use of stereophotogrammetry may be limited due to its field of view, either by the distance required between the two cameras in the stereo-system or by the distance between the structure and the measurement system that does not allow it to capture the entire field of view of interest.

In this case, where the field of view is limited, the measurement could be stepwise, wherein the pair of cameras would be suitable positioned to capture the structure in parts, i.e., from different angles. This, of course, requires repeated assemblies, making it impossible to acquire all points simultaneously in a single measurement setup. The extension of stereophotogrammetry through the use of a multi-camera measurement system is a way of observing the entire structure without the need for repeated assemblies. It can significantly reduce the time and cost of the experiment by measuring all points of interest at once and keeping good spatial resolution of the model.

This possibility of the extension of stereophotogrammetry application through the use of more than one stereo-vision system to capture the entire field of view of interest has been discussed in some papers [5–9]. In the article of Chen et al. [5], the authors use two stereo-systems to create a multi-camera system capable of capturing the entire surface of the structure. The cameras are calibrated in a single coordinate system, so that the multi-camera system obtains the measurements in a common (global) coordinate system, and the process of joining the point clouds of the two stereo-systems is performed using the subset-based matching method adopted in the three-dimensional digital image correlation (3DDIC) technique. A limitation of the technique, in this case, is that the calibration requires that the calibration object can be viewed simultaneously by all cameras, which in some practiced cases can be difficult. In the work of Wang et al. [6], it is also used a multi-camera system and the calibration of each stereo-system is made independently, generating a coordinate system for each stereo-system. Subsequently, the calibration parameters of the stereo-systems are used for the transformation of the independent coordinate system in a common coordinate system. This method has the advantage, in relation with the previous one, of being able to calibrate each stereo-system separately; however, it is necessary to perform the merging of the point clouds using some frame transformation technique.

Currently, stitching techniques have been emerging as an important frame transformation technique used in the 3D object reconstruction. In the most part of the time, they are employed just to achieve the geometry of the model. It recreates the geometry design by merging the point clouds captured by various view positions of the camera and the geometry of the model is obtained in a stepwise way; therefore, the stitching techniques cannot be employed for dynamic measurement, unless ensuring a stead-state excitation condition.

In this work is presented a proposal where stitching techniques, unlike of its most common use (static and stepwise), are employed to perform the alignment of two-point clouds of a structure under dynamic excitation and a comparison of some alignment algorithms is carried out to analyze which one better fits to this purpose. The point cloud registration technique used in the 3D scanning for obtaining the geometry of the model is exploited as a technique for dynamic measurement (displacement) of large structures with high spatial resolution of the model. Three different image registration algorithms, principal component analysis (PCA), singular value decomposition (SVD), and iterative closest point (ICP), are proposed to perform the junction of the point clouds of each stereo-system. The main aspect to be highlighted herein is the use of these algorithms to perform the alignment of the point clouds aiming the application to dynamic measurements, since in the most found articles, these algorithms are used to perform static measurements and the point clouds are captured in a sequential way and not in a single measurement set [10–13]. The proposal is applied to vibration measurement of a wind turbine blade of 2.3 m in length, whose field of view of the whole set of points of interest is greater than the field of view of a unique stereo-vision system. The reconstruction of the set of measured points was obtained from the junction of the points' clouds of each stereo-system like in the article [14], which the authors discuss the feasibility of this approach for operational modal analysis and compare the results with the finite-element model. Herein, is presented a more detailed evaluation of the stitching process trying to quantify the measuring errors. Three different algorithms are evaluated in the stitching process and a probabilistic and statistical analysis of the error generated by the transformation of the point clouds was performed. In a final evaluation, the natural frequencies of the structure obtained from the optical measured data were compared with the values measured with a set of accelerometers.

2 Stitching techniques

Point cloud registration techniques are widely employed to obtain virtual models of real structures. They are used in different fields, such as 3D printing, 3D mapping, 3D object detection, 3D scanning, and others [15, 16]. In the 3D scanning, which this work has been based on, the full reconstruction of structures using multi-camera system requires a reliable and robust image registration algorithm to align the 3D point clouds captured by each camera system to obtain the entire field of view of the whole model, the called stitching process.

The stitching process, in this paper, consists in the realignment of the corresponding point clouds obtained by two independent stereo-camera systems, properly positioned, seeking to obtain, through of the junction of both point clouds, a view of the whole measurement region of the model. In this case, one point cloud is defined as reference point cloud, denominated target point cloud and the other, denominated source point cloud, is reoriented to the target system through the alignment of those paired points in the common area. The alignment is performed using the transformation matrix (rotation and translation) obtained from the set of corresponding points in the common area of both point clouds. In Fig. 1, is shown, schematically, this process.

The stereophotogrammetry measuring technique used in this work is the three-dimensional point-tracking (3DPT) technique. It uses photogrammetric fundamentals to identify the coordinates of discrete points mounted on the structure. A series of optical targets (usually high contrast circular points or retroreflective targets) are mounted on the structure, which are the measuring points. The centers of the optical targets are obtained using an ellipse detection algorithm and the coordinate of the points in the space is calculated using a triangulation technique. The displacements of the points in different stages are defined comparing the values to a reference coordinate, which provides the displacement of the model for those target points. The great interest in its use for structural analysis is that the responses are given at discrete points, which is very similar to pointwise conventional measurement systems (laser and accelerometer sensors). Therefore, the data can readily be adapted to be used in well-established conventional vibration analysis tools with some advantage, since it is possible to obtain a high spatial resolution of discrete points over very large areas.

The use of 3DPT measuring technique is advantageous in the stitching process, because the pairing of the target points of the two-point clouds is immediate; they are already defined in the experimental setup. The identification of the common target points is the same in the two-point clouds. In the following, is presented the algorithms used in the proposed digital image measurement system aiming at measuring of large structures.

2.1 Principal component analysis

Principle components analysis (PCA) is a statistical tool that has found applications in different fields, such as data reduction, image registration, face recognition, and others [17]. It is a powerful tool for compressing data by projecting the data in the direction of their largest variances. The direction of the largest variance corresponds to the eigenvector with the highest eigenvalue. The eigenvector with the highest eigenvalue is the principle component of the data set. Therefore, if the covariance matrixes of two-point clouds differ from identity matrix, a registration algorithm can be employed to align the eigenvectors of covariance matrixes associated with each data set. The main steps to find the transformation matrix to align the different data sets are presented as follows.

Step 1: Centroids of the common points of the two-point clouds.

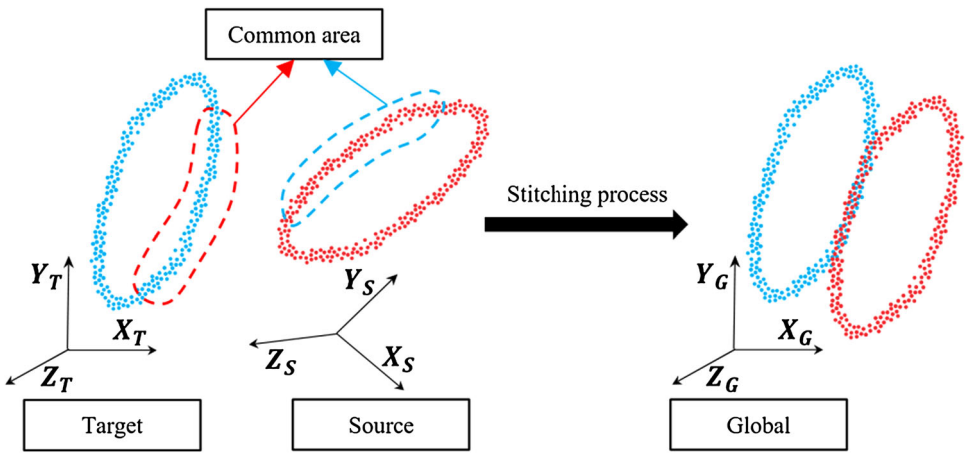

Fig. 1 Stitching process based on the junction of two-point clouds (target and source) located in different coordinate systems (color figure online)

The centroid position of the two-point clouds A and B, $\{\overline{P_A}\} = [\overline{X_A}, \overline{Y_A}, \overline{Z_A}]$ and $\{\overline{P_B} = [\overline{X_B}, \overline{Y_B}, \overline{Z_B}]\}$, is obtained by dividing the sum of all coordinate points, $\{P_{Ai}\} = [X_{Ai} \quad Y_{Ai} \quad Z_{Ai}]$ and $\{P_{Bi}\} = [X_{Bi} \quad Y_{Bi} \quad Z_{Bi}]$, by the number of points in each individual point clouds, Eqs. (1.a) and (1.b):

$$\overline{P_A} = \frac{1}{n}\sum_{i=1}^{n}\{P_{Ai}\} \tag{1.a}$$

$$\overline{P_B} = \frac{1}{n}\sum_{i=1}^{n}\{P_{Bi}\}. \tag{1.b}$$

Step 2: Re-center both sets of common points.

The centroids calculated in step 1 are subtracted from the X, Y, and Z coordinates of all reference points in both data sets, Eqs. (2.a) and (2.b). This procedure removes the translation component of the point clouds, leaving only the rotation to be compensated for

$$[A_{\text{ctr}}] = \begin{bmatrix} X_{A1} - \overline{X_A} & X_{A2} - \overline{X_A} & \cdots & X_{An} - \overline{X_A} \\ Y_{A1} - \overline{Y_A} & Y_{A2} - \overline{Y_A} & \cdots & Y_{An} - \overline{Y_A} \\ Z_{A1} - \overline{Z_A} & Z_{A2} - \overline{Z_A} & \cdots & Z_{An} - \overline{Z_A} \end{bmatrix} \tag{2.a}$$

$$[B_{\text{ctr}}] = \begin{bmatrix} X_{B1} - \overline{X_B} & X_{B2} - \overline{X_B} & \cdots & X_{Bn} - \overline{X_B} \\ Y_{B1} - \overline{Y_B} & Y_{B2} - \overline{Y_B} & \cdots & Y_{Bn} - \overline{Y_B} \\ Z_{B1} - \overline{Z_B} & Z_{B2} - \overline{Z_B} & \cdots & Z_{Bn} - \overline{Z_B} \end{bmatrix}. \tag{2.b}$$

Step 3: Covariance matrix of the mean centered point clouds.

The covariance matrix of the two sets of reference points from the data sets $[A_{\text{ctr}}]$ and $[B_{\text{ctr}}]$ is calculated, Eqs. (3.a) and (3.b):

$$[C_A] = \sum_{i=1}^{n}([P_{Ai}] - [A_{\text{ctr}}]) \times ([P_{Ai}] - [A_{\text{ctr}}])^{\text{T}} \tag{3.a}$$

$$[C_B] = \sum_{i=1}^{n}([P_{Bi}] - [B_{\text{ctr}}]) \times ([P_{Bi}] - [B_{\text{ctr}}])^{\text{T}} \tag{3.b}$$

where $[C_A]$ and $[C_B]$ are orthogonal 3×3 covariance matrices, the diagonal values represent the variances of the data, and the off-diagonal values represent the covariances.
Step 4: Eigenvectors and eigenvalues associated with the covariance matrix of each point cloud.

The eigenvalues and eigenvectors of the covariance matrices $[C_A]$ and $[C_B]$ are calculated. Herein, the eigenvector provides the direction that the data are spread out and the corresponding eigenvalue is a number, indicating how spread out the data is on the corresponding direction. The eigenvector with the largest corresponding eigenvalue gives the direction that the point cloud is the most spread out; thus, the principal component associates with that point cloud, Eqs. (4.a) and (4.b):

$$[V_A, D_A] = \text{eig}(C_A) \tag{4.a}$$

$$[V_B, D_B] = \text{eig}(C_B) \tag{4.b}$$

where D_A and D_B are the corresponding calculated eigenvalues and V_A and V_B are the corresponding eigenvectors of the covariance matrixes A and B.
Step 5: Finding the transformation matrix.

The alignment of the principal components of each point cloud is achieved using the transformation matrix obtained directly from the directions of the eigenvectors. In this case, where $[C_A]$ and $[C_B]$ have their columns as oriented axes, the rotational alignment of the two sets of oriented axes can be calculated using the rotational matrix, Eq. (5):

$$[R] = [V_B] \times [V_A]^{-1} = [V_B] \times [V_A]^{\text{T}}. \tag{5}$$

Step 6: Translation matrix.

Finally, the centroid of the reference data is added to each of the transformed coordinates to translate the aligned and transformed point cloud. By Eqs. 1 and 5, the translation matrix can be calculated, Eq. (6):

$$\{T\} = \{\overline{P_B}\} \times [R] \times \{-\overline{P_A}\}^{\text{T}}. \tag{6}$$

2.2 Singular value decomposition

The singular value decomposition (SVD) is one of the most important tools in numerical linear algebra that has many applications in the field of signal processing and statistics. The SVD of a matrix is its factorization, being it real or complex, into the product of three matrices (U, E, and V), where the columns of U and V are orthonormal and the matrix E is diagonal with positive real entries. The procedure of estimating the transformation matrix using SVD [18] can be broken down into the follow main steps:
Step 1: Centroids of the common points of the two-point clouds.

The centroid of the common points of the two-point clouds is calculated as discussed in the PCA method, Eqs. (1.a) and (1.b).
Step 2: Covariance matrix between the two-point clouds.

The covariance matrix of the two-point clouds is calculated by Eq. (7):

$$[H] = \sum_{i=1}^{n}\left([P_{Ai}] - [\overline{P_A}]\right) \times \left([P_{Bi}] - [\overline{P_B}]\right)^{\text{T}}. \tag{7}$$

Step 3: Optimal rotation matrix.

The optimal rotation matrix values that minimize the root mean squared deviation between two paired sets of points can be calculated using the SVD, Eq. (8):

$$[\sigma] = [U] \times [E] \times [V]^{\mathrm{T}} \tag{8}$$

where $[U]$ and $[V]$ are orthogonal matrices and $[E]$ is a diagonal matrix of singular values. $[\sigma]$, $[U]$, $[E]$, and $[V]$ are all 3×3 matrices. The eigenvectors of $[\sigma][\sigma]^{\mathrm{T}}$ are the columns of $[U]$ and the eigenvectors of $[\sigma]^{\mathrm{T}}[\sigma]$ are the columns of $[V]$. Using the method outlined by Kabsch [19], the orientation of any axis of the rotation matrix can be fixed in the case of reflection. For a proper orientation, the determinant of $[V]$ must be greater than 0, $\mathrm{Det}(\sigma) > 0$; however, if the opposite happens ($\mathrm{Det}(\sigma) \leq 0$), the third column of $[V]$ must be multiplied by -1. Let $[S]$ be the matrix to verify if the orientation of the principal component is correct. Therefore, $[S]$ can be defined according Eq. (9):

$$[S] = \begin{cases} \begin{bmatrix} 1 & 0 & 0 \\ 0 & 1 & 0 \\ 0 & 0 & 1 \end{bmatrix} & \text{if } \mathrm{Det}(\sigma) > 0 \\ \begin{bmatrix} 1 & 0 & 0 \\ 0 & 1 & 0 \\ 0 & 0 & -1 \end{bmatrix} & \text{if } \mathrm{Det}(\sigma) \leq 0 \end{cases}. \tag{9}$$

$[U]$, $[V]$, and $[S]$ provide the necessary information of the rotation matrix and the optimal rotation matrix can be calculated according to Eq. (10):

$$[R] = [V] \times [S] \times [U]^{\mathrm{T}}. \tag{10}$$

Step 4: Translation matrix.

The translation matrix can be calculated as discussed in the PCA method, Eq. (6).

2.3 Iterative closest point

The iterative closest point (ICP) algorithm introduced by Besl and McKay [20] minimizes the difference between the Euclidean distance among the points contained in two-point clouds. The SVD algorithm directly solves the least-square problem that iteratively disregards outliers to improve upon the previous estimate of the rotation and translation parameters. The basis of the procedure to estimate the matrices is shown in Fig. 2.

The algorithm input data are the point cloud used as reference, the called target point cloud (fixed coordinates), and the point cloud to be fitted to the reference point cloud, the called source point cloud. The correspondent points in the common region of both point clouds are defined based on a nearest neighbor approach and a more complex algorithm is used to define these correspondent points using different features, such as color information or geometric shapes. The SVD is used to obtain an initial estimate of the affine transformation matrix that aligns both point clouds. After registration, this whole process is repeated by removing outliers and redefining the point correspondences. Different approaches based on ICP technique can be used to solve the problem, and the technique used in this paper is the ICP point-to-point algorithm.

The ICP point-to-point algorithm was originally described in [21] and it simply obtains the point correspondences by searching for the nearest neighbor target point q_i of a point p_j in the source point cloud. The nearest neighbor matching is defined in terms of the Euclidean distance metric, Eq. (11):

$$\hat{i} = \arg\min_{i} \left\| p_j - q_i \right\|^2 \tag{11}$$

where $i \in [1, 2, \ldots, N]$, and N represents the number of points in the common area of the target point cloud. Like in the SVD approach, the rotation $[R]$ and translation $[t]$ matrices are estimated by minimizing the squared distance between these corresponding pairs, Eq. (12):

$$\hat{R}, \hat{t} = \arg\min_{R,t} \sum_{i-1}^{N} \| (Rp_i + t) - q_i \|^2. \tag{12}$$

The $\hat{R}$ and $\hat{t}$ matrices are obtained iteratively solving Eq. (12).

3 Experimental test

To evaluate the feasibility of the proposal of using the stitching process to extend the capability of the digital image measurement system to measure large structures, it was mounted a test bed of a wind turbine blade. In this context, large structure means that the measured field of view of interest of the model could not be captured by a unique stereo-vision system because of its size. It is necessary to do it in parts or using multi stereo-systems. The blade structure was also instrumented with a set of accelerometers for comparison purpose.

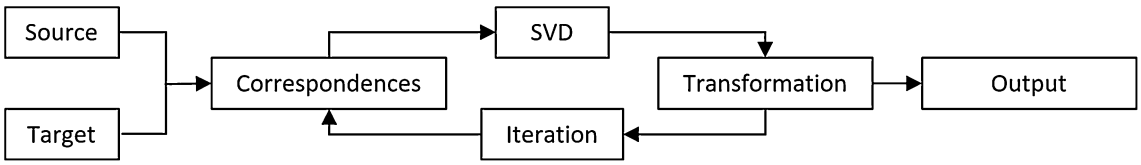

Fig. 2 Schematic of the ICP algorithm

3.1 Experimental setup

The multi-camera experimental setup includes a 2.3-m cantilevered wind turbine blade (Fig. 3) and two stereo-vision systems, composed of four synchronized complementary metal-oxide semiconductor (CMOS) cameras. The multi-camera system is composed of a pair of 12-megapixel cameras (4046 × 3072 pixel CMOS sensor) named stereo-vision A and a pair of 4-megapixel (2048 × 2048 pixel CMOS sensor) PHOTRON high-speed cameras named stereo-vision B, and both stereo-vision systems were equipped with 24-mm lenses.

The stereo-vision system A was placed 1.3-m away from the turbine blade and the stereo-vision system B was placed 1.6 m away from the blade and the fields of view of the cameras contain an overlapped area covered by both stereo-vision systems. In Fig. 4, is shown schematically the view of the two stereo-vision systems, including the common area viewed by both systems. The right half of the blade was covered by the stereo-vision A, while the left one was covered by the stereo-vision B and the common area, at the middle of the blade, was covered by both.

The measuring points were conveniently chosen and identified by a collection of 142 optical targets (measured points) placed on the blade. One part of the structure (104 points) was viewed from the stereo-vision A and the other part (64 points) was viewed from the stereo-vision B. The points viewed by the stereo-vision system A, including the overlap area, are numbered from 1 to 104, in a sequential order, from the top-right corner increasing as it goes down and left. The points located in the overlap area (captured by the two stereo-vision systems) are numbered from 79 to 104 (totalizing 26 points). The points viewed by the stereo-vision system B, including also the overlap area, are numbered from 1 to 64 also in a sequential order, from the top-right corner increasing as it goes down and left. The points located in the overlap area are those numbered from 1 to 26. Hence, the point 79 in the displacement field A corresponds to the point 1 in the displacement field B, the point 80 in the displacement field A corresponds to the point 2 in the displacement field B, and so on.

In addition, to compare the optical measured data with a more well-established technique, the blade was instrumented with a set of 12 triaxial accelerometers. They were conveniently positioned in the structure in such a way that each accelerometer has a corresponding measuring point in the optical system.

4 Stitching results

Two tests were carried out, first, a stationary test for a statistical and probabilistic study of the errors concerning of the alignment and the transformation of the point cloud source to the point cloud target in the stitching process and later, a vibration test of the wind turbine blade. In the first test, the wind turbine blade was in a stationary condition, that means, without any load or motion and in the second test, the blade was excited by an impact input. In Fig. 5, is schematically shown the whole process to obtain the reconstruction of the structure in a common reference system, which involves capturing the structure in separated pieces by the multi-camera system, the obtaining of the transformation matrices, and the stitching of the two-point clouds.

The displacement in the X and Y directions is in-plane (edgewise) displacement and in the Z direction is out-of-plane (flapwise) displacement.

4.1 Stationary test

In the stationary test, the goal was to verify the noise level of the measurement due to the stitching process. The test consisted of capturing a series of images of the blade without loading using two independent stereo-vision systems and applying the stitching techniques to reconstruct the structure and to obtain the displacement field of all points in a common reference system. The points of the

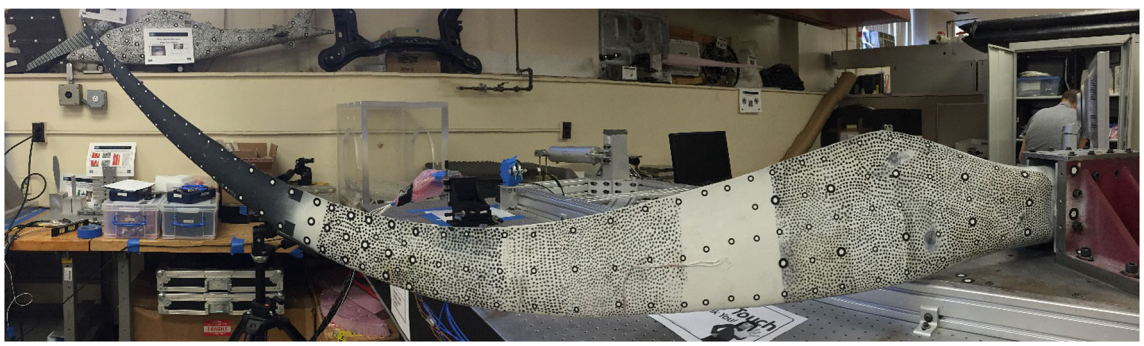

Fig. 3 2.3-m cantilevered wind turbine blade and the location of the 142 optical targets. The counting starts from the top-right corner and increases as it goes down (color figure online)

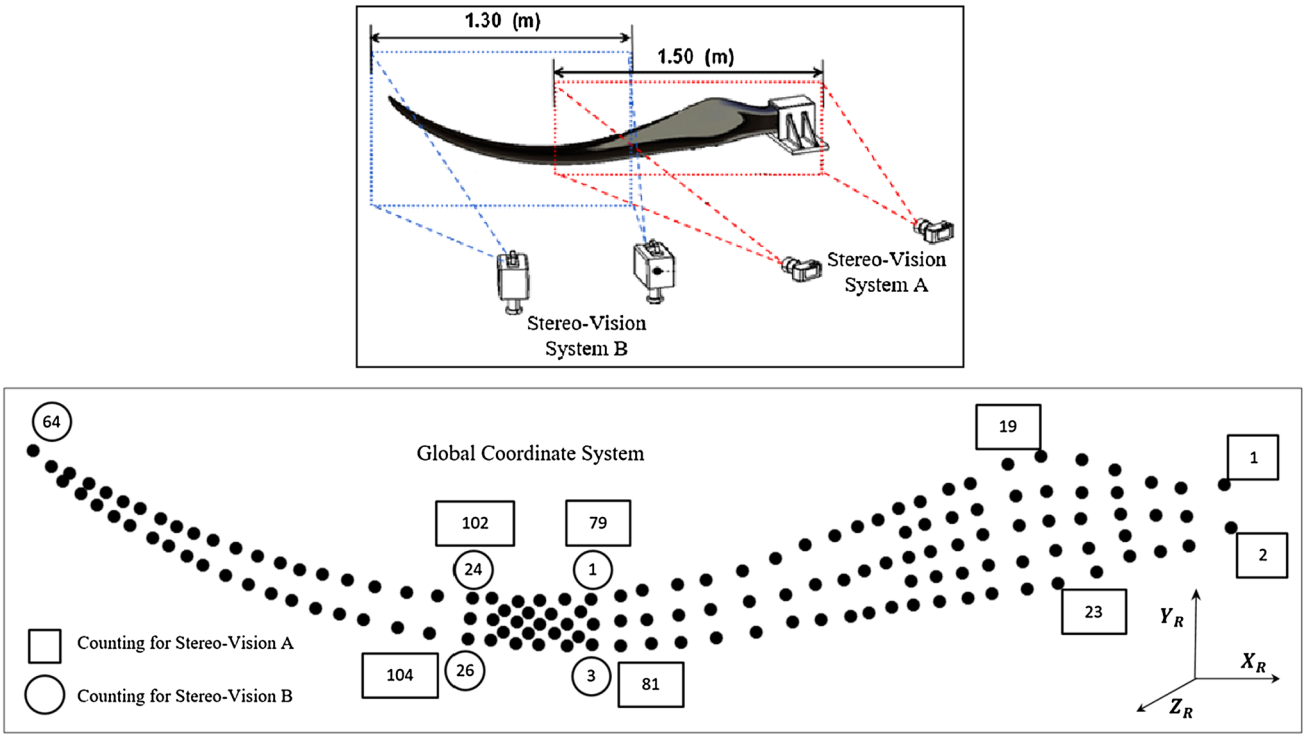

Fig. 4 Multi-camera setup with the two-synchronized stereo-vision systems and their respective fields of view (color figure online)

point cloud B (source), measured in the overlap area, were transformed to the reference system A (target) and compared with their corresponding points measured directly in the reference system A. In this case, the position of the points must be equal (null displacement), since the structure is stopped without any loading.

The measurement was repeated several times to have an evaluation of the repeatability of the data. 50 frames of the blade were captured and the displacement of the set of target points of field A and field B, in their own coordinate system, was estimated using the 3DPT technique (PONTOS software). The key issue in this case is that the stereo-vision systems were calibrated in their own coordinate system. Therefore, the two-point clouds need to be reoriented in a common system. Herein, this was carried out by the stitching technique. In the stitching process, the two-point clouds were alignment and jointed in reference coordinate system using the PCA, SVD, and ICP proposed algorithms. The process was performed considering that the displacement field A was the reference system and the points from the overlapped area of the two fields of view were used to obtain the transformation matrices to move the points of field B to the reference field A. Once the realignment of those points of field B to the reference system was obtained, the displacement points of field B, in the reference system (field A), were estimated. The displacements were measured in the three directions, in the in-plane direction, X and Y and in the out-of-plane direction, Z. The discussion of the results presented here focuses only the out-of-plane direction measuring, since, in the stereophotogrammetry, it is assumed that the measuring in the out-of-plane direction is three times more inaccurate than in-plane directions [22, 23].

In Fig. 6, are shown the histograms, as well as the estimated probability density functions of the measured data at point 3. It is possible to see that the functions present a shape of a Gaussian distribution, which would be used to provide the estimation of the expected errors limits in the measurement for such measuring setup. The results shown in Fig. 6a refers to the use of the PCA algorithm transformation, in Fig. 6b refers to the SVD, and in Fig. 6c refers to the ICP. The standard deviations were, respectively, 0.0133, 0.0133, and 0.0149 mm.

In this stationary test (zero displacement of the structure), the errors in the measuring might be related to the stitching process and to the optical system noise level. The obtained errors are in the order of hundredth of millimeters. Assuming that the measuring points will stay in a limit of $\pm 1\ \sigma$ from the mean, the largest expected error in the measuring process will be ± 0.0133, ± 0.0133, and ± 0.0149 mm, respectively, for the use of PCA, SVD, and ICP algorithms.

The same analysis was carried out for all measuring points in the overlapped area and the results presented the same pattern behavior.

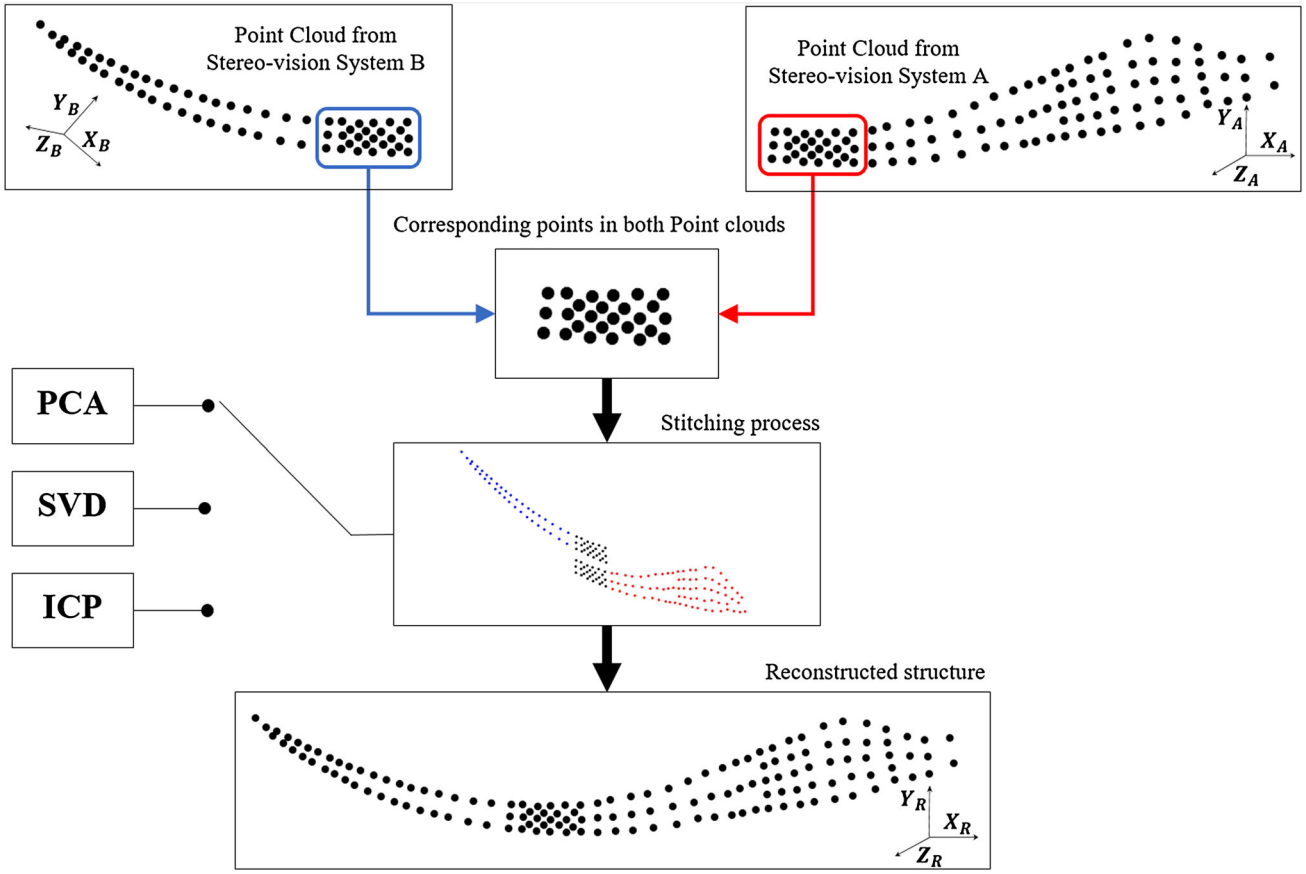

Fig. 5 Whole stitching process, views of the displacement fields of the stereo-visions A and B, the proposed algorithms to perform the alignment and the view of the reconstructed structure (color figure online)

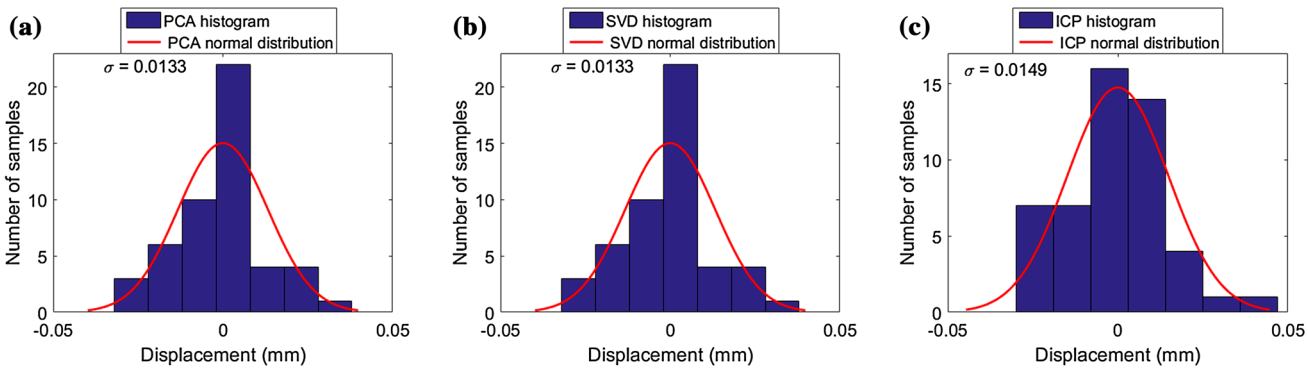

Fig. 6 Histogram and distribution curve of the point 3 (displacement field B) for **a** PCA, **b** SVD and **c** ICP registration techniques (color figure online)

4.2 Dynamic test

In this test, the goal was to access the capability of the proposal for measuring the vibration of the turbine blade under a dynamic loading condition. The multi-camera system captured the motion of the structure using a sample rate of 96 frames per second. The total time of acquisition was defined by the total available memory in the cameras, which provided 19 s of recording, leading to a total of 1829 frames. The structure was excited with an impact hammer in the *Z* direction at the point 104. The point cloud A was used as reference system (target) and the point cloud B (source) was aligned to the reference system.

The blade also was instrumented with a set of accelerometers to comparison propose. The software LMS was used to control the acquisition system, and it was used a frequency sample of 128 Hz, block size of 4096 points, and 10 averages. It was used triaxial accelerometers,

sensitivity of 100 mv/g. The positioning of accelerometers in the back part of blade was done taking into account the position of the optical targets, to keep a corresponding equivalence among them. An instrumented impact hammer was used to excite the structure, in the back part of the blade close to accelerometer number 8. Figure 7 illustrates a sketch of the location of the optical measured points and the accelerometers on the blade.

The data from the two-point clouds captured by stereo-vision systems from the field of view A and from the field of view B were processed in a similar way to that used in the previous analysis. Like in the static test, initially, it is presented a discussion of the measured data at points 3 and 81, in the out-of-plane direction. In Fig. 8, is shown the plot of the displacement signal of point 81, directly measured in the reference system and its corresponding in field B, point 3.

A quantitative comparison of the displacements of the two points was done using the time response assurance criterion (TRAC). In this criterium, TRAC values close to 1.0 indicate very good similarities and values close to 0.0 indicate minimal or no similarity between the time traces. The TRAC value obtained for this analysis is given by Eq. (13):

$$\mathrm{TRAC}_{ji} = \frac{\left[\{X1_j(t)\}^{\mathrm{T}}\{X2_i(t)\}\right]^2}{\left[\{X1_i(t)\}^{\mathrm{T}}\{X1_i(t)\}\right]\left[\{X2_j(t)\}^{\mathrm{T}}\{X2_j(t)\}\right]} = 0.99. \quad (13)$$

In Fig. 9, is shown the difference of the two displacement signals taking the displacement signal of the point 81 as reference. They present a mean difference value of 0.0130 mm and standard deviation of 0.0232 mm.

Finally, the same analysis comparison was carried out for all other points in the overlap area. In Table 1, are presented the maximum and the mean difference of the RMS values, as well as, the corresponding points at which they happen. In the first column, are presented the maximum errors which point it occurs for the in-plane and out-of-plane measurement and in the second is presented the average error. The results show that the out-of-plane displacement error, taking the values of the point cloud A (directly measured) as reference, was not greater than 66.1 μm, and it occurred in point 22 (corresponding to point 100). The PCA and SVD algorithms gave a more precise result than ICP, although the difference was not significant.

In a second step, the results of the optical measuring system were compared with the conventional measuring system using accelerometers. The comparison was not made, directly, comparing the signals, but comparing the natural frequencies of the model. In the bandwidth analyzed, 0–40 Hz were found four peaks of frequencies in the spectrum of both signals, from the optical and the accelerometer measuring systems. In Table 2, is shown the first four frequencies measured with the accelerometers system (accelerometer 1), the optical system (target point 61), and the difference of them, taking the accelerometer as reference.

The analysis of the measurement results showed that in the static test, assuming limit of $\pm 2\ \sigma$, the largest estimated error is $\pm$ 0.0298 mm. In the dynamic test, the results were evaluated comparing the signals measured in the overlapped area. The signals measured directly in the reference system (point cloud A) were compared with their equivalents in the point cloud B, transformed to the reference system. The TRAC criterion indicates good similarities among them. The greatest average difference found among the signals, taking the point cloud A as reference, was 0.0661 mm.

The probabilistic and statistical analysis of the error due to the transformation of the point clouds discussed in this paper have shown that the stitching process is a promising tool for structural displacement measurement. It presented equivalence to the usual system using accelerometers.

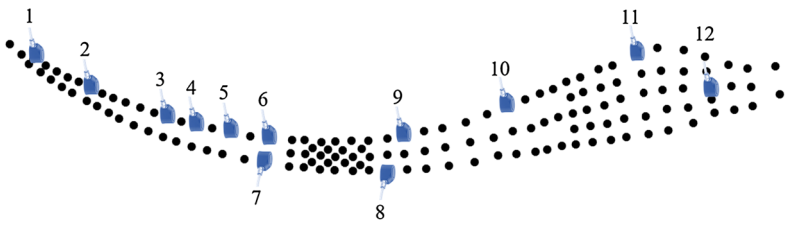

Acc.	Optical
1	139
2	129
3	117
4	113
5	109
6	105
7	106
8	78
9	73
10	58
11	24
12	11

Fig. 7 Sketch of the accelerometers position and optical targets (color figure online)

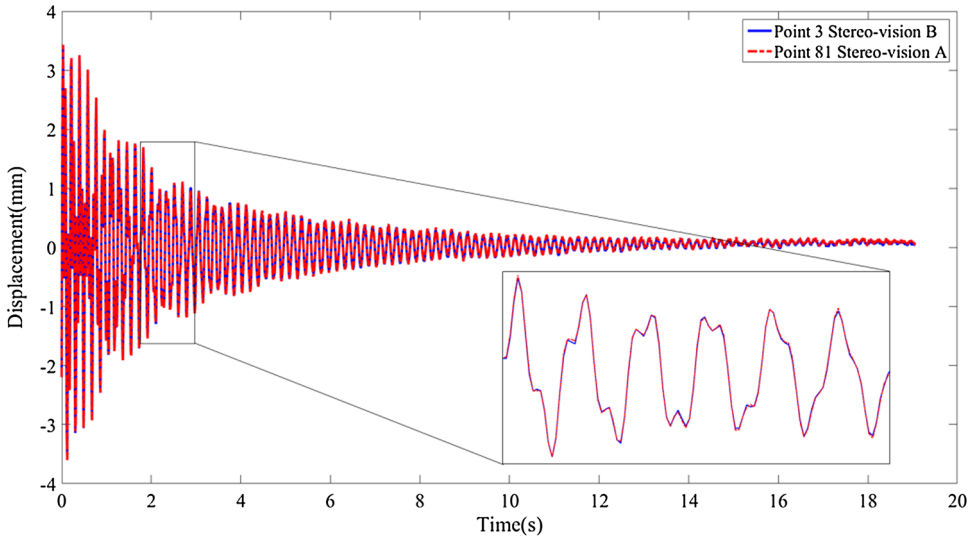

Fig. 8 Comparison of the out-of-plane displacements between the corresponding points 81 (stereo-vision A) and 3 (stereo-vision B) when the blade is impacted with an impact hammer. It was captured 1829 image stages (color figure online)

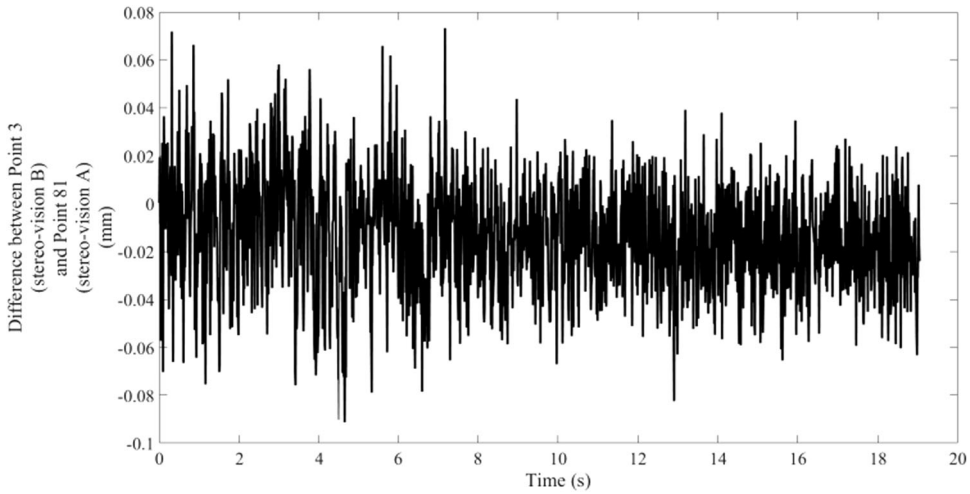

Fig. 9 Difference in the displacements of points 81 (reference) and 3 (point cloud B)

Table 1 Difference between the out-of-plane and in-plane displacements of the common points in the overlapped area are quantified

	Error								
	RMS (max.)						RMS (average)		
	X	Point	*Y*	Point	*Z*	Point	*X*	*Y*	*Z*
PCA	0.0208	3	0.0293	21	0.0638	22	0.0187	0.0282	0.0489
SVD	0.0209	3	0.0292	21	0.0639	22	0.0187	0.0281	0.0490
ICP	0.0238	26	0.0345	21	0.0661	22	0.0188	0.0331	0.0507

The maximum and the average error values for each coordinate and the corresponding points are shown

5 Final remarks

The work presents a discussion of a three-dimensional point tracking (3DPT) measuring approach for measurement of large structures in which the entire field of interest could not be captured by a unique stereo-vision system. Two pairs of a stereo-system were used to capture the whole field of measurement interest of the model and three different point cloud registration algorithms, PCA, SVD and ICP, were used in the stitching process of the point clouds.

To obtain the geometry of the structure using stitching techniques in the form of point clouds, these point clouds were stitched together by the proposed algorithms. Unlike of its most common use (static and stepwise measurement), this work presented stitching techniques to perform the

Table 2 Blade frequencies using accelerometers and multi-camera systems

Frequencies	Accelerometers (Hz)	Optical (Hz)	Diff. (%)
1	5.59	5.66	1.25
2	15.97	15.95	0.13
3	25.88	26.25	1.42
4	36.39	36.37	0.05

alignment of two-point clouds of a wind turbine blade under dynamic excitation.

The proposed approach was evaluated to measure the vibration of a wind turbine blade of 2.3 m in length. The reconstruction of the full set of measured points was obtained from the junction of the points clouds of each stereo-system in a common reference system. The analyses of the obtained data for the static and the dynamic measuring condition showed that the three used algorithms give compatible results. It can be seen that the PCA and SVD algorithms obtained a more precise result than ICP, although the difference was not significant. The measured frequencies of the model were also compared with the ones measured using accelerometers and the results have been shown very promising, which show to be an interesting option for vibration and modal analysis application of large-scale structures, with great possibility of application for operational modal analysis.

References

1. Sutton M, Wolters W, Peters W, Ranson W, McNeill S (1983) Determination of displacements using an improved digital correlation method. Image Vis Comput 1:133–139
2. Sutton M, Mingqi C, Peters W, Chao Y, McNeill S (1986) Application of an optimized digital correlation method to planar deformation analysis. Image Vis Comput 4:143–150
3. Chu TC, Ranson WF, Sutton MA (1985) Applications of digital-image-correlation techniques to experimental mechanics. Exp Mech 25:232–244
4. Baqersad J, Poozesh P, Niezrecki C, Avitabile P (2016) Photogrammetry and optical methods in structural dynamics—a review. Mech Syst Signal Process. https://doi.org/10.1016/j.ymssp.2016.02.011
5. Chen F, Chen X, Xie X, Feng X, Yang L (2013) Full-field 3D measurement using multi-camera digital image correlation system. Opt Lasers Eng 51:1044–1052
6. Wang Y, Lava P, Coppieters S, Houtte PV, Debruyne D (2013) Application of a multi-camera stereo DIC set-up to assess strain fields in an Erichsen test: methodology and validation. Strain 49:190–198
7. Malesa M, Malowany K, Kujawińska M (2014) Multi-camera DIC system with a spatial data stitching procedure for measurements of engineering objects. Photonics Lett Pol 6:157–159
8. Nguyen TN, Huntley JM, Burguete RL, Coggrave CR (2012) Multiple-view shape and deformation measurement by combining fringe projection and digital image correlation. Strain 48:256–266
9. LeBlanc B, Niezrecki C, Avitabile P, Chen J, Sherwood J (2013) Damage detection and full surface characterization of a wind turbine blade using three-dimensional digital image correlation. Struct Health Monit 12:430–439
10. Barone S, Paoli A, Razionale AV (2012) Three-dimensional point cloud alignment detecting fiducial markers by structured light stereo imaging. Mach Vis Appl 23:217–229
11. Rusu RB, Blodow N, Beetz M (2009) Fast Point Feature Histograms (FPFH) for 3D registration. IEEE Int Conf Robot Autom 2009:3212–3217
12. Li N, Cheng P, Sutton MA, McNeill SR (2005) Three-dimensional point cloud registration by matching surface features with relaxation labeling method. Exp Mech 45:71–82
13. Wang F, Ye Y, Hu X, Shan J (2016) Point cloud registration by combining shape and intensity contexts. In: 2016 9th IAPR workshop on pattern recognition in remote sensing (PRRS), pp 1–6
14. Poozesh P, Baqersad J, Niezrecki C, Avitabile P, Harvey E, Yarala R (2016) Large-area photogrammetry based testing of wind turbine blades. Mech Syst Signal Process. https://doi.org/10.1016/j.ymssp.2016.07.021
15. Urbanic RJ, ElMaraghy HA, ElMaraghy WH (2008) A reverse engineering methodology for rotary components from point cloud data. Int J Adv Manuf Technol 37:1146–1167
16. Keaveney S, Keogh C, Gutierrez-Heredia L, Reynaud EG (2016) Applications for advanced 3D imaging, modelling, and printing techniques for the biological sciences. In: 2016 22nd international conference on virtual system & multimedia (VSMM), pp 1–8
17. Smith LI (2002) A tutorial on principal components analysis. Cornell University, Ithaca, pp 51–65
18. Bellekens B, Spruyt V, Berkvens R, Weyn M (2014) A survey of rigid 3d pointcloud registration algorithms. In: Fourth international conference on ambient computing, applications, services and technologies. Citeseer, pp 8–13
19. Kabsch W (1978) A discussion of the solution for the best rotation to relate two sets of vectors. Acta Crystallogr 34:827–828
20. Besl PJ, McKay ND (1992) A method for registration of 3-D shapes. Pattern Anal Mach Intell IEEE Trans 14:239–256
21. Rusu RB (2010) Semantic 3D object maps for everyday manipulation in human living environments. KI Künstliche Intelligenz 24:345–348
22. PONTOS v6.3. GOM mbH, Braunschweig, 2011
23. ARAMIS v6.3. GOM mbH, Braunschweig, 2011